Giant saltation on Mars

Murilo P. Almeida[†], Eric J. R. Parteli[†], José S. Andrade, Jr.[†‡§], and Hans J. Herrmann[†‡]

[†]Departamento de Física, Universidade Federal do Ceará, 60455-900, Fortaleza, CE, Brazil; and [‡]Computational Physics, Institut für Baustoffe, Eidgenössische Technische Hochschule Zürich, Schafmattstrasse 6, 8093 Zurich, Switzerland

Edited by H. Eugene Stanley, Boston University, Boston, MA, and approved March 11, 2008 (received for review January 9, 2008)

***Saltation*, the motion of sand grains in a sequence of ballistic trajectories close to the ground, is a major factor for surface erosion, dune formation, and triggering of dust storms on Mars. Although this mode of sand transport has been matter of research for decades through both simulations and wind tunnel experiments under Earth and Mars conditions, it has not been possible to provide accurate measurements of particle trajectories in fully developed turbulent flow. Here we calculate the motion of saltating grains by directly solving the turbulent wind field and its interaction with the particles. Our calculations show that the minimal wind velocity required to sustain saltation on Mars may be surprisingly lower than the aerodynamic minimal threshold measurable in wind tunnels. Indeed, Mars grains saltate in 100 times higher and longer trajectories and reach 5-10 times higher velocities than Earth grains do. On the basis of our results, we arrive at general expressions that can be applied to calculate the length and height of saltation trajectories and the flux of grains in saltation under various physical conditions, when the wind velocity is close to the minimal threshold for saltation.**

aeolian transport | critical phenomena | turbulent flows | granular flows | particle-laden flows

As on Earth, the primary mode of aeolian transport on Mars is *saltation* (1–5)—particles are first lifted off from the surface and accelerated downwind, next colliding with the ground and ejecting new particles (6–12)—which is responsible, among other things, for the appearance of sand dunes and ripples such as those recently imaged at Meridiani Planum on Mars (Fig. 1). However, two mechanisms compete for making saltation on Mars very different from what it is on Earth: (*i*) Martian conditions require 10 times higher wind velocities than Terrestrial ones (13, 14), being seen only a few times a decade during gusts of extreme aeolian activity (2, 3, 5, 15–19); and (*ii*) the lower gravity and stronger winds of Mars allow particles, once in the air, to fly higher and to remain longer in the atmosphere, being accelerated by the wind more than they are on Earth (8, 20). From wind tunnel experiments under low-pressure conditions that reproduce the density of the Martian air, we could already gain some flavor of the efficiency of such high-speed saltating particles in dislodging sand grains or raising dust when colliding onto Martian soils (4). However, very little is known quantitatively about the saltation trajectories, grain velocities, and sand flux.

One fundamental question is how much sand a Martian wind of given strength can transport in saltation. As the number of particles ejected from the grain-bed collisions ("splash") and launched into the air increases, the wind loses more momentum until the number of saltating grains per unit area and per unit time, the sand flux, achieves a saturated value, q_s (6–8, 10, 11, 21, 22). However, saltating grains modify the profile of the wind, which loses part of its momentum to accelerate the particles (7). This interaction, which strongly affects the trajectories of the particles, could never be calculated in simulations. Only the trajectory of *one* single grain, just after it starts moving from rest, being lifted off by the wind, could be estimated numerically (8, 20).

The simulation of Martian saltation in the steady state (at saturation) in the turbulent wind is performed by using an approximate $(\kappa - \varepsilon)$ model for the turbulent wind field, which has been introduced in a previous article (23). In the model, the turbulent wind flow is calculated inside a wind channel without particles, and once a stable profile is achieved, particles are injected into the channel. The particles are submitted to gravity and drag, and particle motion is calculated, taking into account the interactions between the grains and the air. The calculations of ref. 23 have shown how the interaction between the fluid and the particles distorts the wind profile within the saltation layer and led to a scaling law for the saturated flux as function of the wind speed when it is close to the minimal value for sand transport (23). In the present work, the model is applied to study saltation transport on Mars and to calculate the dependence of the grain velocities, the impact angles, and the height and the length of the saltation trajectories on the wind shear velocity when the sand flux is in the steady state.

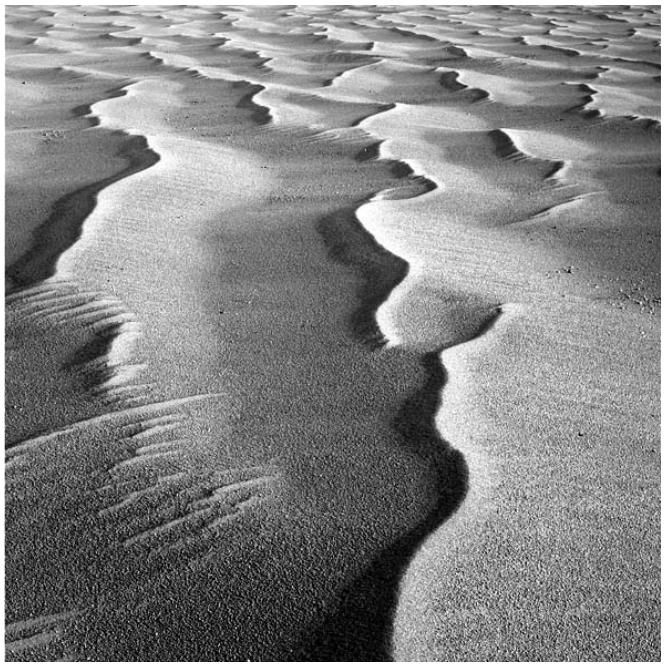

Fig. 1. Sand ripples imaged by the Opportunity rover across the plain known as Meridiani Planum on Mars. Image credit: National Aeronautics and Space Administration/Jet Propulsion Laboratory.

This paper is organized as follows. After a summary of the simulation procedure given in the next section, our results are presented and discussed. We compare results obtained for saltation on Mars and on Earth and introduce a set of general equations that can be applied to calculate saltation flux and grain trajectories in various physical environments. Finally, the for-

Author contributions: M.P.A., E.J.R.P., J.S.A., and H.J.H. designed research, performed research, analyzed data, and wrote the paper.

The authors declare no conflict of interest.

This article is a PNAS Direct Submission.

[§]To whom correspondence should be addressed. E-mail: soares@fisica.ufc.br.

mation of dust storms under present Mars conditions is explained on the basis of the simulation results and an interpretation of aeolian processes on Mars is proposed.

The Model

The numerical simulations of saltation consist of solving, first, the turbulent wind field inside a long two-dimensional channel (wind tunnel) and, next, the air feedback with the dragged particles. The details of the calculation procedure are described elsewhere (23). The fluid (air) is incompressible and Newtonian, the Reynolds-averaged Navier–Stokes equations with the standard $\kappa - \varepsilon$ model being used to describe turbulence [the FLUENT (Fluent) commercial package of fluid dynamics is used in this study].

Wind Flow and Particle Transport. The turbulent wind is, first, calculated without particles. The wind is generated by a pressure difference imposed between the extremities of the tunnel (23) and achieves a stable profile, the wind velocity $u(z)$ increasing with the height z as $u(z) = 2.5u_*\log z/z_0$, where z_0 is the surface roughness ($\approx 10^{-4}$ m) and u_*, the wind shear velocity, quantifies the wind strength (6). Boundary conditions are zero wind velocity at the bottom wall and zero shear ($u_* = 0$) at the upper wall (gravity $\boldsymbol{g}$ points downward).

Once steady-state turbulent flow is produced, particles are injected from the inlet at the ejection angle of grain-bed collisions with a velocity of the order of 60 cm/s. Grain trajectories are obtained by integrating the equation of motion:

$$\frac{d\boldsymbol{v}_p}{dt} = F_D(\boldsymbol{u} - \boldsymbol{v}_p) + \boldsymbol{g}(\rho_p - \rho_{fluid})/\rho_p, \qquad [1]$$

where $\boldsymbol{v}_p$ is the particle velocity, ρ_{fluid} and ρ_p are the density of the fluid and of the particles, respectively, and $F_D(\boldsymbol{u} - \boldsymbol{v}_p)$ represents the drag force per unit particle mass, where

$$F_D = \frac{18\eta}{\rho_p d^2}\frac{C_D \mathrm{Re}}{24}, \qquad [2]$$

$\mathrm{Re} = \rho_{fluid} d|\boldsymbol{u} - \boldsymbol{v}_p|/\eta$ is the particle Reynolds number, d is the grain diameter, and η is the air viscosity, and the drag coefficient C_D is taken from empirical relations (24). The feedback on the local velocity of the fluid because of its momentum exchange with the particles is accounted for by adding the momentum change of every particle as it passes through a control volume (23),

$$\boldsymbol{F} = \sum_{\text{particles}} F_D(\boldsymbol{u} - \boldsymbol{v}_p)\dot{m}_p \Delta t, \qquad [3]$$

where $\dot{m}_p$ is the mass flow rate of the particles and Δt is the time step. Each time a particle hits the ground it loses a fraction $r = 0.40$ of its momentum and a new stream of particles is ejected at that position with the ejection angle characteristic of saltation particles, $\theta_{eje} = 36°$ (9, 25). The number of particle streams released, n_p, defines the sand flux $q = \dot{m}_p n_p$. Particle trajectories increase in height with the downwind position, achieving a maximum after a distance ΔL, called "saturation length" (26), from the inlet. The saturated flux, q_s, is identified by the maximum number of particle streams, n_p, that a wind of given strength u_* can transport without flux reducing due to energy loss of the trajectories (23).

Earth and Mars Simulations. In simulations for Earth, gravity $g = 9.81$ m/s^2, air viscosity $\eta = 1.78 \times 10^{-5}$ kg/m·s, and density $\rho_{fluid} = 1.225$ kg/m^3 are taken, and particle diameter $d = 250$ μm and density $\rho_p = 2{,}650$ kg/m^3 are as from sand of terrestrial dunes (6). For Mars we use air density and viscosity $\rho_{fluid} = 0.02$ kg/m^3, respectively $\eta = 1.3 \times 10^{-5}$ kg/m·s, and gravity is $g = 3.71$ m/s^2, and Martian particles have diameter $d = 600$ μm and density

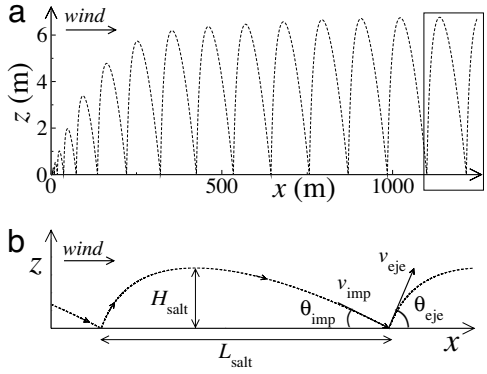

Fig. 2. Typical particle trajectory. (*a*) The dashed line represents the trajectory of one saltating grain calculated by using parameters for Mars with a wind strength of $u_* = 1.78$ m/s. Gravity points downward (negative z direction) and the particle moves downwind, i.e., from left to right. In the absence of the saltating particles, the wind strength increases logarithmically with the height. However, the wind profile is disturbed by the saltating grains as shown in ref. 23. (*b*) Typical saltation trajectory obtained in the calculations—the dashed line corresponds to the saltation path enclosed by the box in *a*—showing the velocity and angle of impact (v_{imp}, θ_{imp}) and of ejection (v_{eje}, θ_{eje}). The length L_{salt} and the maximum height H_{salt} of a saltation trajectory are also indicated.

$\rho_p = 3{,}200$ kg/m^3 typical of Martian dunes sand (27). Simulations are performed with u_* values between 0.27 m/s and 0.5 m/s for Earth and 1.12 m/s and 1.78 m/s for Mars, which means wind velocity values in the range $u = 6.21$–11.5 m/s (Earth) and $u = 25.8$–41.0 m/s (Mars) at a height of 1 m. Taking the wind velocity at this height, the fluid Reynolds number $\mathrm{Re}_f = ud\rho_{fluid}/\eta$ considered in the simulations is in the range 106.8–197.9 for Earth and 23.8–37.8 for Mars.

Whereas Earth trajectories achieve the maximum height after typically $\Delta L = 10$ m, Mars trajectories stabilize after $\Delta L = 1.0$ km (Fig. 2*a*), independently of u_*. Thus, the wind tunnel used in the simulations for Mars is much larger than the one used for Earth simulations (which has length 30 m and height 1.0 m), the former being 2.0 km long with a height of 10 m. We have performed simulations using channels of larger dimensions, both for Mars and for Earth. In both cases, it was found that increasing the size of the tunnel does not change the results. All grain trajectories analyzed in the numerical study are taken from the downwind second half of the tunnel, i.e., where grain trajectories are stabilized. A typical grain trajectory in the steady state obtained in the simulations is shown in Fig. 2*b*, which displays the main elements of saltation that are studied in the present work.

Results and Discussion

Fig. 3 shows the increase of the resulting maximum flux of particles in saltation, q_s, with the shear velocity u_* on Mars. For comparison, the same simulations were performed by using terrestrial atmospheric conditions and grain size and density characteristic of dunes on Earth (Fig. 3 *Inset*).

The scaling of the saturated flux with the shear velocity is universal: $q_s \propto (u_* - u_{*t})^\alpha$, where $\alpha \approx 2.0$ is independent of the atmospheric conditions, and u_{*t}, the *impact threshold* wind velocity—the minimal wind velocity required to sustain the motion of saltating grains at saturation (6)—obtained in the simulations is $\approx$1.12 m/s and 0.26 m/s on Mars and on Earth, respectively. As shown in a previous article (23), we have found a rather good agreement between the data obtained from our simulations for Earth and those obtained from field measurements by Lettau and Lettau (21), thus confirming the validity of our simulation procedure (23).

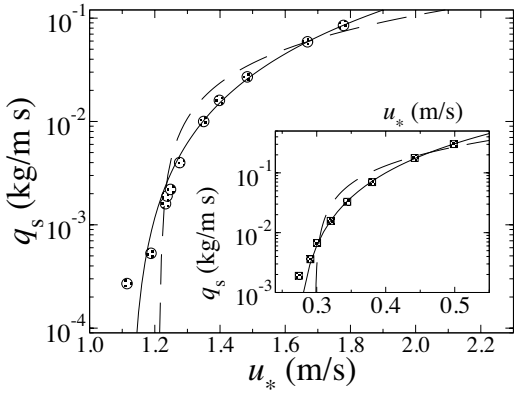

Fig. 3. In the main plot, the circles show the saturated flux q_s calculated as function of the shear velocity u_* for Mars. The quadratic relation $q_s \propto (u_* - u_{*t})^2$, indicated by the solid line, fits the data notably better than the classical equation for planetary sand flux (8), whose corrected version reads (28) $q_w = C[\rho_{fluid}/g]u_*^3(1 - u_{*t}/u_*)(1 + u_{*t}/u_*)^2$ (dashed line), and gives $u_{*t} = 1.12$ m/s for Mars. The range of shear velocities $u_* = 1.12$–1.78 m/s used for Mars corresponds to shear stress $\tau = \rho_{fluid}u_*^2$ values in the range 0.025–0.063 kg/m·s^2. The corresponding calculations for Earth are shown in the *Inset*. In this case, simulations were performed with shear velocities in the range $u_* = 0.27$–0.5 m/s, which corresponds to shear stress values in the range $\tau = 0.089$–0.306 kg/m·s^2.

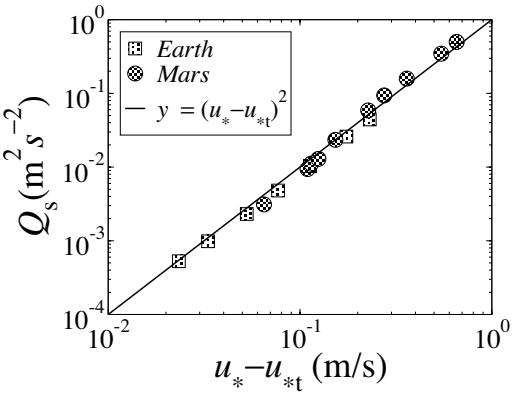

Fig. 4. Normalized flux Q_s defined as $q_s/[227.3 \cdot u_{*t} \cdot d\rho_{fluid}^{5/3}/\eta g^{2/3}]$. Circles and squares correspond to calculations made for Mars and Earth, respectively. The straight line corresponds to the equation $y = (u_* - u_{*t})^2$.

The sand flux depends not only on the wind velocity but also on gravity and atmospheric and sand properties, which must be included in the coefficient of the scaling between q_s and u_*. One expression for $q_s(u_*)$ that includes gravity and atmospheric density was proposed and validated through wind tunnel experiments under Earth and Mars air pressure conditions (8). The simulations of the present work, however, reveal that the air viscosity also plays a relevant role in saltation, and cannot be neglected. If the ratio ρ_{fluid}/g is encoded in the coefficient of $q_s(u_*)$ (8), then dimensional analysis requires a further term with units of velocity to be included into the scaling relation of Fig. 3. As a first guess, the threshold velocity u_{*t} is used. However, it is not possible to find a common proportionality constant for the scaling $q_s \propto [\rho_{fluid}/g]u_{*t}(u_* - u_{*t})^2$ that satisfies both Mars and Earth data. Universality is obtained only when the nondimensional quantity d/l_ν, where the length-scale $l_\nu = (\nu^2/g)^{1/3}$ defines, together with the time-scale $t_\nu = (\nu/g^2)^{1/3}$ the characteristic velocity $v_\nu = l_\nu/t_\nu$, with $\nu = \eta/\rho_{fluid}$ (11), is incorporated into the prefactor of the sand flux equation. This quantity encodes the information of the amount of momentum lost because of the grain-bed collisions that has to be compensated by the drag force in the equilibrium (22). A formula for the sand flux is then obtained, which can be applied to calculate q_s as function of u_* under arbitrary physical environments (Fig. 4):

$$q_s \approx 227.3 \cdot [d\rho_{fluid}/(\nu g)^{2/3}] \cdot u_{*t} \cdot (u_* - u_{*t})^2. \qquad [4]$$

One important lesson for future experiments of sand transport under extraterrestrial conditions follows, therefore, from the simulations: it is not strictly correct to adjust air pressure only to obtain the desired air density (4, 8). Both pressure *and* temperature must be tuned to obtain both air density *and* viscosity of the environment the simulation aims to reproduce. In previous wind tunnel experiments (8) the air pressure in the tunnel was adjusted to reproduce the density of Martian air (CO_2 at $T =$ 200K and $P = 0.75$ kPa), whereas the simulations were performed under Earth gravity. We have performed a fit to the simulation data by using the classical sand flux expression by White (8), where we used the corrected equation $q_w = C[\rho_{fluid}/g]u_*^3(1 - u_{*t}/u_*)(1 + u_{*t}/u_*)^2$ (28). We could not find a universal constant C, whereas the fit to the simulation data (dashed line in the main plot and in the *Inset* of Fig. 3) gives $C \approx 2.9$ for Mars and $C \approx 18$ for Earth. We find that the constant C must be replaced by $A_w[d/l_\nu]$, where the constant $A_w \approx 19$ seems to be universal, to predict correctly the sand flux under different temperature and pressure conditions.

Indeed, not only is it relevant to know the saturated flux but also it is important to estimate how long a given gust of saltation can last on Mars (2, 3, 5). The minimum shear velocity u_{*ft} required to entrain particles *directly* into the air, which is measurable in wind tunnels (6, 13, 14), has a well understood dependence on the particle size and density, on gravity, on the atmospheric density, on the internal friction between particles, and on interparticle cohesion, the last factor being most relevant for the smallest (dust) particles (14). Once u_* exceeds u_{*ft} and saltation begins, particle entrainment succeeds mainly through particle–soil collisions, and, thus, the wind velocity required to sustain saltation, u_{*t}, is somewhat smaller than u_{*ft}. The ratio of the impact threshold velocity u_{*t}—obtained in the simulations of the present work—to the measured aerodynamic threshold u_{*ft} on Mars appears different from what it is on Earth. Whereas a ratio u_{*t}/u_{*ft} of $\approx$0.96 is found in the simulations of saltation on Earth, the Martian u_{*t}/u_{*ft} is much smaller, $\approx$0.48. Wind shear velocities of $\approx$2.5 m/s are required to start saltation of sand on Mars (14), but once saltation is initiated, the high trajectories and large grain velocities (Fig. 5) enable Martian saltation to be sustained at much more realistic values of u_*, around just 1.0 m/s.

The length L_{salt} and the maximum height H_{salt} of the trajectories of saltating grains on Mars and on Earth are shown in Fig. 5. At large values of u_*, L_{salt} seems to scale with u_*^2, whereas H_{salt} increases nearly linearly with u_*. The faster growth of L_{salt} with u_* is attributed to the larger acceleration saltating particles with higher trajectories experience. However, both the length and height of the saltation paths increase linearly with the shear velocity u_*, when this is close to the threshold (Fig. 6). Dimensional analysis leads to a scaling of H_{salt} and L_{salt} with $t_\nu(u_* - u_{*t})$. Using our data to obtain the respective constants of proportionality, we find that universal equations for L_{salt} and H_{salt} can be obtained if the quantity $\sqrt{l_\nu/d}$ is incorporated into the coefficients of both saltation length and height. In this manner, we arrive at the following expressions, which can be used to predict the saltation trajectories on an arbitrary planetary surface, for u_* close to the threshold u_{*t}:

$$H_{salt} \approx 81.46 \cdot (\nu^2/g)^{1/3} \cdot (u_* - u_{*t})/\sqrt{gd}\,, \qquad [5]$$

$$L_{salt} \approx 1091.5 \cdot (\nu^2/g)^{1/3} \cdot (u_* - u_{*t})/\sqrt{gd}\,, \qquad [6]$$

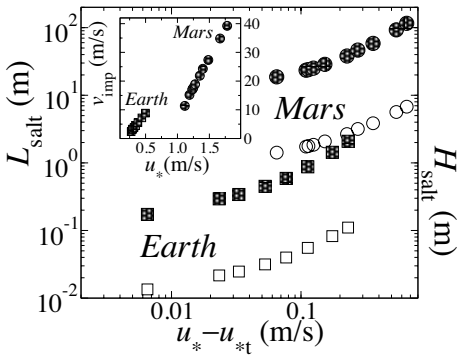

Fig. 5. Giant grain trajectories on Mars. The main plot shows the mean length L_{salt} (filled symbols) and height H_{salt} (open symbols) of the saltation trajectories on Mars (circles) and Earth (squares) as a function of $u_* - u_{*t}$, where $u_{*t} = 1.12$ m/s for Mars and 0.267 m/s for Earth as from Fig. 3. The *Inset* shows the impact velocities v_{imp} of Mars (circles) and Earth (squares) saltating grains as a function of u_*.

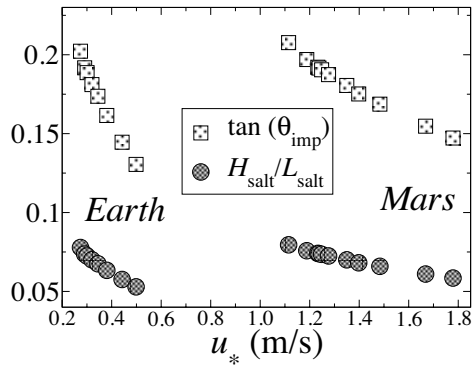

Fig. 7. The shape of saltation trajectories. Both the impact angle θ_{imp} [squares represent tan(θ_{imp})] and the ratio H_{salt}/L_{salt} (circles) decrease with u_* because particle acceleration increases with the wind shear velocity.

where $(\nu^2/g)^{1/3}$ is the characteristic lengthscale l_ν and $\sqrt{gd}$ represents the grain velocity necessary to escape from the sand bed (11).

As compared with Earth trajectories, Martian saltation paths are giant. Whereas Earth saltating particles do not exceed heights of 15 cm, maximum heights reached by particles saltating under typical sand-moving winds on Mars (Fig. 2) amount to 1–5 m. Moreover, Martian grains saltate in 20- to 120-m-long paths—such particles appear suspended when seen in a wind tunnel with length of a few meters (8). The simulation results are in agreement with the expectation that the saltation length L_{salt} should scale with the quantity $L_{drag} = d\rho_p/\rho_{fluid}$, which is a characteristic length that encodes the information of the inertia of a saltating grain in the surrounding fluid (29). Substituting the parameter values for Mars ($d = 600$ μm, $\rho_{fluid} = 0.02$ kg/m^3, $\rho_p = 3{,}200$ kg/m^3) and for Earth ($d = 250$ μm, $\rho_{fluid} = 1.225$ kg/m^3, $\rho_p = 2{,}650$ kg/m^3), we find $L_{drag} =$ 96 m on Mars and 54 cm on Earth, which appear consistent with the typically two order of magnitude higher values of L_{salt} on Mars as obtained in the simulations.

Because of the lower gravity and higher acceleration of Martian saltating grains, the first grain trajectories (just after saltation begins) on Mars are flatter than on Earth, as found in previous calculations (20). However, the situation is different when saltation is fully developed. In the steady state, under the same relative wind shear velocity, the shape of the grain trajectories (the ratio L_{salt}/H_{salt}) on Mars is the same as on Earth (Fig. 7). Martian impact angles at saturation are also similar to the terrestrial ones, but the impact velocity of saltating grains on Mars is nearly 5–10 times higher than on Earth.

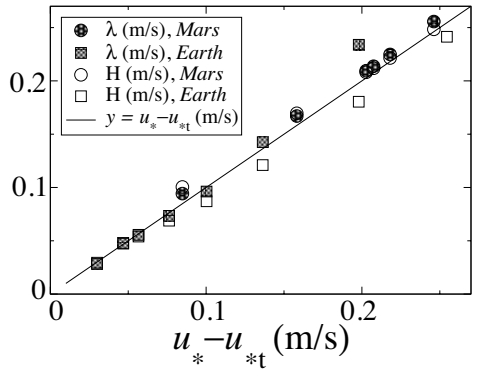

Fig. 6. Universal expressions for saltation transport. The normalized length $\lambda \equiv L_{salt}/[1091.5\cdot(l_\nu/\sqrt{gd})]$ and height $H \equiv H_{salt}/[81.46\cdot(l_\nu/\sqrt{gd})]$ as function of $u_* - u_{*t}$, are shown by the filled and open symbols, respectively, both for Mars (circles) and Earth (squares), with $u_{*t} = 1.03$ and 0.244 m/s for Mars and for Earth, respectively. All data seem to follow the straight line, $y = u_* - u_{*t}$.

Dune Formation on Mars. How can the simulation results presented here be helpful for the understanding of dune formation on Mars? Whether dunes could be formed at present atmospheric conditions of Mars remained an open question for decades since the first images of Mars dunes taken by Mariner 9 (1, 30). Noticeable changes on the surface of a few Martian dunes have been detected only recently (e.g., as reported in refs. 17 and 31). These observations provided evidence that dunes can be formed and move on the present Mars. However, because the wind velocity is seldom above the threshold for saltation motion on Mars, the rate at which changes on the dunes occur is so low that no dune migration could be detected from orbiters up to now.

The migration velocity of Mars dunes can be calculated from two pieces of information: the first one is the frequency at which sand-moving winds occur on Mars; the second is the sand flux obtained from the simulations of the present work. A dune of stationary shape under a wind of constant strength u_* blowing steadily from the same direction migrates with velocity $v_d \approx aQ_s/V^{1/3}$ (6), where V is the dune volume, $Q_s \equiv q_s/\rho_{sand}$, the bulk density of the sand being defined as $\rho_{sand} = 0.62\rho_p \approx 2{,}000$ kg/m^3, and $a \approx 15$ from field measurements of terrestrial dunes (32). Indeed, as shown by Mars missions, saltation transport on Mars occurs occasionally, at intervals of approximately $\Delta T = 5$ years (2, 3, 5, 17). Moreover, Arvidson *et al.* (2) and Moore (3) calculated that each gust of saltation transport probably lasts for about $\Delta t = 40$ s. This information allows one to define the fraction $f = \Delta t/\Delta T$ of time during which saltation transport occurs on Mars: $f \approx 2.54 \times 10^{-7}$. In this manner, the migration velocity of Martian dunes can be obtained with the equation

$$v_d = [f\, a\, \rho_{sand}^{-1}]q_s/V^{1/3} \approx 1.9\cdot 10^{-9} q_s/V^{1/3}, \qquad [7]$$

where q_s is a function of u_* and can be obtained from the results of Fig. 3. For example, let us assume that, as on Earth, sand-moving winds at Martian dune fields have typical strength $u_* \approx 1.5\, u_{*t}$ (33, 34), which gives $u_* \approx 1.62$ m/s. From Fig. 3, this corresponds to $q_s \approx 0.063$ kg/m·s or $2.0\cdot 10^6$ kg/m·year. Under such conditions, a small Martian dune displaying length and width $\approx$100 m, which has a volume of $\approx$20,000 m^3 (35), moves at a rate of $\approx$0.00014 m/year, and needs, therefore, $\approx$7,000 years to move 1.0 m, according to Eq. **7**.

However, we remark that it is not possible to generalize this result for all Martian dunes, because the frequency with which saltation events occur on Mars may vary in a significant way with the geographical location. As recently observed by Fenton (17),

this frequency may vary even within a given location, in such a manner that while no changes on the surface of some dunes in a given dune field may occur in a time span of over 5 terrestrial years, other dunes in the same field may migrate in the same period at a rate as high as 0.5–1.0 cm/year (17). Moreover, whereas dune motion on the north polar region of Mars is inhibited during the winter seasons by the carbon dioxide frost that forms on the surface of the dunes, the sand of dunes in several other locations on Mars appears indurated, possibly because of the presence of salts, in such a way that these dunes do not move at all (19). In this manner, provided no induration is present and the frequency and duration of the gusts of winds above threshold at a given place on Mars are known, then the results of Fig. 3 can be applied to obtain the migration velocity of sand dunes on Mars.

Dust Storms on Today's Mars. It is not surprising that the sporadic dust storm events of Mars are mostly associated with events of sand saltation (2, 3, 5). The giant trajectories and large impact velocities of Martian saltating grains make saltation an efficient means for raising dust into the atmosphere of Mars (4). Direct entrainment of dust by air shear requires much stronger winds than those required for moving sand (36), but once saltation initiates, the new threshold for dust transport is the impact threshold for saltation, u_{*t}. Although the threshold for sand entrainment is very infrequently exceeded (2), values comparable to the impact threshold $u_{*t} \approx 1.0$ m/s obtained in our calculations may occur often on the Martian surface (16). This frequency leads to a new view of aeolian transport on Mars. For a storm of Martian dust to start, wind only needs to lift off a bit of sand, igniting saltation. Uncommon values of wind strength $\approx$2.5 m/s capable of moving sand (13, 14) must be of course reached at least within a rapid gust of aeolian activity. But no matter if, after such a gust, the wind strength decreases to typical Martian values, $\approx$1.0 m/s (16), dust will not cease spreading into the air—as long as sand saltates on Mars.

In conclusion, the present article reports the calculation of particle trajectories in a turbulent wind. The sand flux and saltation height and length on Mars and on Earth were studied and general expressions (Eqs. **4**, **5**, and **6**) were found that can be applied to calculate these quantities under different physical conditions, e.g., on the surface of Venus or Titan. The giant saltation trajectories and the high grain velocities on Mars are the missing link to understand the triggering of dust storms under typical wind velocities $u_* \approx 1.0$ m/s at present conditions of Mars (4).

The large values of impact velocities obtained in the simulations allow us to understand the high erosion of Martian soils during the rare gusts of sand transport as predicted from wind tunnel simulations of saltation under low-pressure conditions that reproduce the density of the Martian air (4) and from experiments of particle–bed collisions under typical conditions of grain velocity on Mars.[¶] In a recent report (35), it has been shown that the larger splash events on Mars compared with the Earth reduce the transient of flux saturation on Mars as predicted from the scaling of dunes with the length of saltation trajectories (6). It would be interesting to extend the calculations of the present work to study the development of saltation from the initiation of transport by aerodynamic (direct) entrainment, with inclusion of a splash function that accounts for the response of the number of ejected grains with respect to the impact velocity of saltating particles.

[¶]Marshall JR, Borucki J, Bratton C, Aeolian sand transport in the planetary context: Respective roles of aerodynamic and bed-dilatancy thresholds. 29th Lunar and Planetary Science Conference, March 16–20, 1998, Houston, TX, abstr 1131.

ACKNOWLEDGMENTS. We acknowledge J. P. Merrison, K. S. Edgett, and R. Sullivan for fruitful discussions. This work was supported in part by the Conselho Nacional de Pesquisas (CNPq), the Comissao de Aperfeiçoamento de Pessoal de Nival Superior (CAPES), the Fundação Cearense de Amparo à Pesquisa (FUNCAP), the Volkswagenstiftung, and the Max-Planck Prize.

1. McCauley JF (1973) Mariner 9 Evidence for wind erosion in the equatorial and mid-latitude regions of Mars. *J Geophys Res* 78:4123–4137.
2. Arvidson RE, Guinness EA, Moore HJ, Tillmann J, Wall SD (1983) Three Mars years: Viking Lander 1 imaging observations. *Science* 222:463–468.
3. Moore HJ (1985) The Martian dust storm of Sol 1742. *J Geophys Res* 90:163–174.
4. Greeley R (2002) Saltation impact as a means for raising dust on Mars. *Planet Space Sci* 50:151–155.
5. Sullivan R, *et al.* (2005) Aeolian processes at the Mars Exploration Rover Meridiani Planum landing site. *Nature* 436:58–61.
6. Bagnold RA (1941) *The Physics of Blown Sand and Desert Dunes* (Methuen, London).
7. Owen PR (1964) Saltation of uniformed sand grains in air. *J Fluid Mech* 20:225–242.
8. White BR (1979) Soil transport by winds on Mars. *J Geophys Res* 84:4643–4651.
9. Anderson RS, Haff PK (1988) Simulation of eolian saltation. *Science* 241:820–823.
10. Butterfield GR (1993) in *Turbulence: Perspectives on Flow and Sediment Transport*, eds Clifford NJ, French JR, Hardisty J (Wiley, New York), pp 305–335.
11. Andreotti B (2004) A two-species model of aeolian sand transport. *J Fluid Mech* 510:47–70.
12. Merrison JP, *et al*. (2005) Sand and dust transport on Mars. *Geophys Res Abstr* 7:04679.
13. Greeley R, Leach R, White B, Iversen JD, Pollack J (1980) Threshold windspeeds for sand on Mars: Wind tunnel simulations. *Geophys Res Lett* 7:121–124.
14. Iversen JD, White BR (1982) Saltation threshold on Earth, Mars and Venus. *Sedimentology* 29:111–119.
15. Sutton JL, Leovy CB, Tillman JE (1978) Diurnal variations of the Martian surface layer meteorological parameters during the first 45 sols at two Viking Lander sites. *J Atmos Sci* 35:2346–2355.
16. Sullivan R, *et al*. (2000) Results of the imager for Mars Pathfinder windsock experiment. *J Geophys Res* 105:24547–24562.
17. Fenton LK (2006) Dune migration and slip face advancement in the Rabe Crater dune field, Mars. *Geophys Res Lett* 33:L20201, 10.1029/2006GL027133.
18. Jerolmack DJ, Mohrig D, Grotzinger JP, Fike, DA, Watters WA (2006) Spatial grain sizes sorting in eolian ripples and estimation of wind conditions on planetary surfaces: Application to Meridiani Planum, Mars. *J Geophys Res* 111:E12S02, 10.1029/2005JE002544.
19. Schatz V, Tsoar H, Edgett KS, Parteli EJR, Herrmann HJ (2006) Evidence for indurated sand dunes in the Martian north polar region. *J Geophys Res* 111:E04006, 10.129/2005JE002514.
20. White BR, Greeley R, Iversen JD, Pollack JB (1976) Estimated grain saltation in a Martian atmosphere. *J Geophys Res* 81:5643–5650.
21. Lettau K, Lettau H (1978) in *Exploring the World's Driest Climate*, eds Lettau H, Lettau K (Univ. of Wisconsin, Madison), pp 110–147.
22. Durán O, Herrmann HJ (2006) Modellization of saturated sand flux. *J Stat Mech* P07011.
23. Almeida MP, Andrade JS, Jr, Herrmann HJ (2006) Aeolian transport layer. *Phys Rev Lett* 96:018001.
24. Morsi SA, Alexander AJ (1972) An investigation of particle trajectories in two-phase flow systems. *J Fluid Mech* 55:193–208.
25. Rioual F, Valance A, Bideau D (2000) Experimental study of the collision process of a grain on a two-dimensional granular bed. *Phys Rev E* 62:2450–2459.
26. Kroy K, Sauermann G, Herrmann HJ (2002) Minimal model for sand dunes. *Phys Rev Lett* 88:054301.
27. Edgett KS, Christensen PR (1991) The particle size of Martian aeolian dunes. *J Geophys Res* 96:22765–22776.
28. Greeley R, Blumberg DG, Williams SH (1996) Field measurements of the flux and speed of wind-blown sand. *Sedimentology* 43:41–52.
29. Andreotti B, Claudin P, Douady S (2002) Selection of dune shapes and velocities Part 1: Dynamics of sand, wind and barchans. *Eur Phys J B* 28:321–339.
30. Breed CS, Grolier MJ, McCauley JF (1979) Morphology and distribution of common 'sand' dunes on Mars: Comparison with the Earth. *J Geophys Res* 84:8183–8204.
31. Bourke MC, Edgett K, Cantor BA (2008) Recent aeolian dune change on Mars. *Geomorphology* 94:247–255, 10.1016/j.geomorph.2007.05.012.
32. Hersen P, *et al*. (2004) Corridors of barchan dunes: Stability and size selection. *Phys Rev E* 69:011304.
33. Fryberger SG, Dean G (1979) in *A Study of Global Sand Seas*, ed McKee ED (U.S. Geological Survey, Washington, DC) p 137.
34. Embabi NS, Ashour MM (1993) Barchan dunes in Qatar. *J Arid Environ* 25:49–69.
35. Parteli EJR, Herrmann HJ (2007) Dune formation on the present Mars. *Phys Rev E* 76:041307.
36. Iversen JD, Pollack JB, Greeley R, White BR (1976) Saltation threshold on Mars: The effect of interparticle force, surface roughness, and low atmospheric density. *Icarus* 29:381–393.